Centrality dependence of charged-particle pseudorapidity distributions from d+Au collisions at $\sqrt{s_{NN}} = 200$ GeV

I. Arsene[10], I. G. Bearden[7], D. Beavis[1], C. Besliu[10], B. Budick[6], H. Bøggild[7], C. Chasman[1], C. H. Christensen[7], P. Christiansen[7], J. Cibor[3], R. Debbe[1], E. Enger[12], J. J. Gaardhøje[7], M. Germinario[7], K. Hagel[8], H. Ito[1,11], A. Jipa[10], J. I. Jørdre[9], F. Jundt[2], C. E. Jørgensen[7], R. Karabowicz[4], E. J. Kim[1,11], T. Kozik[4], T. M. Larsen[12], J. H. Lee[1], Y. K. Lee[5], S. Lindal[12], R. Lystad[9], G. Løvhøiden[12], Z. Majka[4], A. Makeev[8], M. Mikelsen[12], M. Murray[8,11], J. Natowitz[8], B. Neumann[11], B. S. Nielsen[7], D. Ouerdane[7], R. Płaneta[4], F. Rami[2], C. Ristea[10], O. Ristea[10], D. Röhrich[9], B. H. Samset[12], D. Sandberg[7], S. J. Sanders[11], R. A. Sheetz[1], P. Staszel[4,7], T. S. Tveter[12], F. Videbæk[1], R. Wada[8], Z. Yin[9], I. S. Zgura[10]
(BRAHMS Collaboration)

[1] Brookhaven National Laboratory, Upton,New York 11973, [2] Institut de Recherches Subatomiques and Université Louis Pasteur, Strasbourg, France, [3] Institute of Nuclear Physics, Krakow, Poland, [4] Jagiellonian University, Krakow, Poland, [5] Johns Hopkins University, Baltimore, Maryland 21218, [6] New York University, New York, New York 10003, [7] Niels Bohr Institute, University of Copenhagen, Denmark, [8] Texas A&M University, College Station,Texas 77843, [9] University of Bergen, Department of Physics, Bergen,Norway, [10] University of Bucharest,Romania, [11] University of Kansas, Lawrence, Kansas 66045, [12] University of Oslo, Department of Physics, Oslo,Norway

(Dated: Jan. 21, 2004)

Charged-particle pseudorapidity densities are presented for the d+Au reaction at $\sqrt{s_{NN}} = 200$ GeV with $-4.2 \leq \eta \leq 4.2$. The results are shown for minimum-bias events and 0-30% and 30-60% central events. The data were obtained using several subsystems of the BRAHMS experiment at RHIC. Models incorporating both soft physics and hard, perturbative QCD-based scattering physics agree well with the experimental results. The data do not support predictions based on strong-coupling, semi-classical QCD. A comparison of the central 200 GeV data with full-overlap d+Au results at $\sqrt{s_{NN}} = 19.4$ GeV shows similar behavior in the near-fragmentation regions after accounting for the number of participants of the respective fragments.

PACS numbers: 25.75.Dw

The saturation of initial parton densities in relativistic heavy-ion collisions, a manifestation of high-density QCD, is expected to significantly influence the pseudorapidity and centrality dependence of the emitted charged-particle densities from these reactions [1–5]. Some of the earliest results from the Relativistic Heavy-Ion Collider (RHIC) have been charged-particle pseudorapidity density distributions for Au+Au collisions [6–11]. While these data have been used to constrain model predictions for ultrarelativistic heavy-ion collisions, they have been inconclusive as to whether parton saturation in the initial state contributes significantly to the reaction dynamics. Calculations that include these saturation effects are successful in describing the earlier Au+Au results [3, 4]. Equally good agreement is found, however, with calculations that do not include saturation effects but rather focus on the energy-loss mechanisms for the multiple minijets created in the collisions [12–15]. Kharzeev, Levin and Nardi [5] have suggested that a study of light-particle on heavy ion d+Au collisions might result in a significantly stronger signature and hence might help to select among different models of the reaction dynamics.

We report on a measurement of the charged-particle pseudorapidity densities for the d+Au reaction at $\sqrt{s_{NN}} = 200$ GeV with pseudorapidity η coverage of $-4.2 \leq \eta \leq 4.2$. The pseudorapidity densities are reported for minimum-bias events and 0-30% and 30-60% central events. The results allow for a detailed comparison to model predictions of particle production at RHIC energies. The most central data (0-30%) correspond to a situation where both deuteron nucleons are expected to participate in the reaction. This allows for an interesting comparison with full-overlap d+Au data obtained by the NA35 collaboration at $\sqrt{s_{NN}} = 19.4$ GeV [16].

The present analysis employs several of the BRAHMS global detector subsystems: The Si Multiplicity Array (SiMA) and the scintillator Tile Multiplicity Array (TMA) [17] are used for centrality determination and to measure the pseudorapidity densities close to mid-rapidity. The Beam-Beam Counter (BBC) arrays are used to reconstruct the collision vertex and to determine the pseudorapidity densities at larger pseudorapidities. The "Inelasticity Counters" (INEL), developed for the pp2pp experiment [18], are used for a close to minimum-bias experiment trigger and to provide vertex position information in cases where the beam-beam counter arrays are not able to establish the vertex location. Full details of the BRAHMS apparatus can be found in ref. [19].

The layout of the SiMA and TMA detectors for the d+Au experiment is similar to that presented for earlier measurements of Au+Au multiplicities at $\sqrt{s_{NN}} = 130$ GeV and 200 GeV, and details of the analysis procedures can be found in refs. [9, 10]. The SiMA was configured with 25, 4 cm × 6 cm Si wafers in an hexagonal ar-

rangement around the beam pipe, with each wafer functionally divided into 7 discrete segments along the beam line and located 5.3 cm from the beam axis. Four sides of the hexagonal array were populated with six detectors, each. To accommodate forward- and mid-rapidity spectrometers (see ref. [19]), the remaining two sides were left largely unpopulated with the exception of a single wafer mounted on the forward-spectrometer side of the array away from the forward angles. The TMA was populated with 38, 12 cm $\times$ 12 cm plastic scintillator tiles with fibre-optic readout located 13.7 cm from the beam axis. The hexagonal TMA array had four sides fully populated with eight detectors, each. The mid-rapidity and forward spectrometer sides were populated with two and four detectors, respectively. With this arrangement, the SiMA and TMA can each measure pseudorapidity densities with $-2.2 \leq \eta \leq 2.2$ using an extended range of collision vertex locations z about the nominal array center, with -35 cm $\leq$ z $\leq$ 35 cm. Particle multiplicities were deduced for the individual SiMA and TMA elements by using GEANT [20] simulations to convert the observed energy-loss signals in the individual detector elements to the number of primary particles hitting that element. The HIJING event simulator [12] was used to obtain the primary mix of particle types and momenta.

Two Beam-Beam Counter arrays are used to extend coverage out to $\eta = \pm 4.2$, with each array consisting of a set of Cherenkov UV-transmitting plastic radiators coupled to photomultiplier tubes. The arrays are positioned around the beam pipe on either side of the nominal interaction point at a distance of 2.20 m. By timing the leading particles hitting the two arrays, a vertex position resolution of $\approx$ 2 cm was achieved. Charged-particle multiplicities are deduced from the number of particles hitting each detector, as found by dividing the measured ADC signal by that corresponding to a single incident particle.

Three pairs of INEL Counters were used to develop a near-to-minimum bias trigger by detecting charged particles in the pseudorapidity range $3.2 < |\eta| < 5.3$. The basic INEL counter consists of a plastic scintillator ring that is segmented into four pieces and arranged about the beam pipe. The counters corresponding to the innermost utilized pair are located on either side of the nominal interaction vertex at $\pm$155 cm. These counters have an inner radius of 4.13 cm and an outer radius of approximately 12.7 cm, with flat regions introduced at the outer radius to allow for the mounting of phototubes. On the positive pseudorapidity side, two scintillator pieces are removed to accommodate the forward spectrometer. The other four counters have inner radii of 6.67 cm and outer radii of approximately 12.7 cm, again with flat regions at the outer radius. These counters are paired at $\pm$416 cm and $\pm$660 cm. Using the relative time-of-flight of particles hitting the left and right arrays in coincidence it is possible to determine the interaction vertex with a resolution of $\approx$ 5 cm. The INEL counters are also used to provide a minimum-bias trigger for the experiment and,

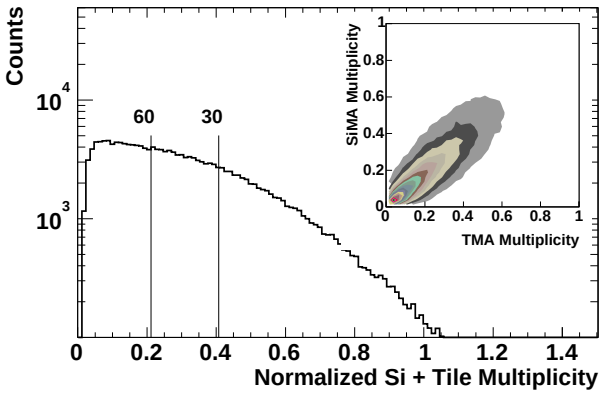

FIG. 1: SiMA and TMA averaged multiplity distribution normalized to the 1% centrality level. Centrality limits of 30% and 60% are indicated. The insert shows the correlation between the SiMA and TMA multiplicities.

based on GEANT simulations, are believed to be sensitive to 92% of the total reaction cross section.

Reaction centrality is determined using a geometry-weighted average of SiMA and TMA multiplicities. Both the SiMA and TMA multiplicities are corrected for the distance of the actual interaction vertex from the nominal vertex at array center. GEANT simulations were used to correct for the possibility that neither the SiMA nor the TMA detectors will be hit by a particle for the most peripheral events.

Figure 1 shows the normalized SiMA and TMA averaged multiplicities. The shape is very different from that found for the corresponding Au+Au spectrum[9] where there is an extended "flat" region and a well-defined high multiplicity knee. This difference reflects in part the overall lower particle multiplicities for the d+Au measurement and the correspondingly larger event-by-event scatter of the number of measured particles relative to the average number of particles observed for a given centrality selection. This is seen, for example, by comparing the individual multiplicities in the SiMA and TMA as shown in the Fig. 1 insert. The width of the correlation band reflects the statistical scatter of the semi-independent multiplicity measurements. Reaction centralities are found by integrating the yield under the multiplicity curve. Limits for the 30% and 60% centrality cuts are indicated by the vertical lines.

Figure 2 shows the resulting charged-particle pseudorapidity-density plots for minimum-bias events and 0-30% and 30-60% central events. The SiMA and TMA results have been averaged. Overall statistical uncertainties are indicated or are smaller than the data points. Systematic uncertainties, denoted by the horizontal brackets, are determined by exploring the variation of the deduced pseudorapidity densities to reasonable changes in the energy calibrations and background subtraction. Our results agree within systematic uncertainties with recently reported results

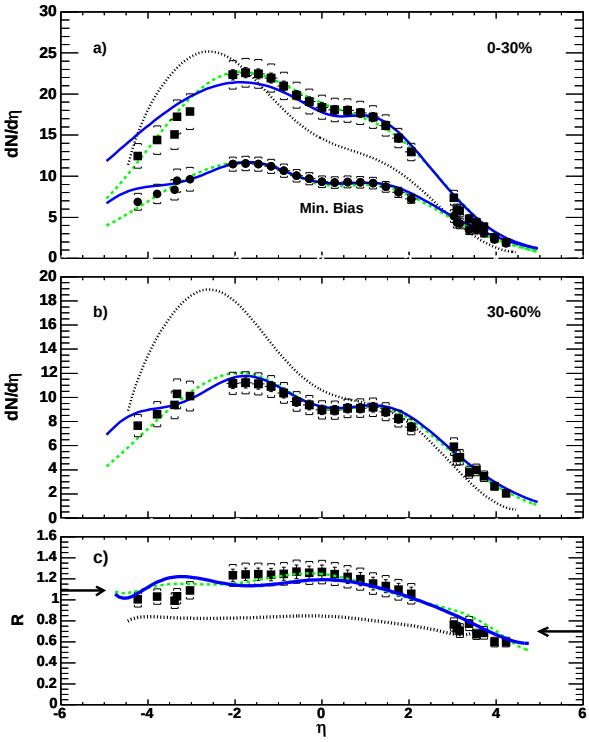

FIG. 2: Charged-particle multiplicities for a) minimum-bias and 0-30% central events and b) 30-60% central events. c) Scaled multiplicity ratio R, as discussed in the text. The left (right) arrows show corresponding values for Au- (d-) participant scaling. Statistical uncertainties are indicated by vertical lines or are smaller than the symbols. Detached horizontal brackets indicate the total (statistical and systematic) uncertainties. The dashed, solid and dotted curves are the results of the HIJING, AMPT and Saturation models, respectively.

of the PHOBOS Collaboration [21], although we see a more rapid fall-off with increasing pseudorapidity on the Au fragmentation side.

Three model calculations are compared to the data. The dashed curves show the predictions of the HIJING model [12]. HIJING is a Monte Carlo model that includes both soft and hard, perturbative QCD-based scattering effects. The solid curves show the predictions of the AMPT model [13–15] which includes both initial partonic and final hadronic interactions. The centrality selections for the HIJING and AMPT models were done by selecting the fraction of events with the highest particle multiplicity within the pseudorapidity range of the SiMA and TMA arrays. Both models do very well in reproducing the experimental results at midrapidity and at positive rapidities leading to the deuteron fragmentation region. At negative rapidity leading to the Au fragmentation region the two models start to diverge and here HIJING appears in slightly better agreement with our results.

The dotted curves in Fig. 2 show the expectations of the QCD Saturation Model [5]. In this case the centrality dependence was based on the published curves of charged-particle pseudorapidity densities for different centrality ranges given in ref. [5]. The Saturation Model accounts for the high-density QCD effects that are expected to limit the number of partons in the entrance channel. The model predicts more pronounced effects in the d+Au system as compared to the Au+Au system, where good agreement was found with the data. However, the model appears to be unsuccessful in the d+Au system at reproducing either the centrality or pseudorapidity dependence of the results.

Fig. 2c shows the ratio R ($= 0.62 \times dN/d\eta(0-30\%)/dN/d\eta(30-60\%)$) of pseudorapidity distributions for the 0-30% and 30-60% data, where 0.62 is the ratio of the number of participants for the peripheral and central data as found using HIJING. Uncorrelated systematic uncertainties of 5% are assumed for the measurements. Model calculations based on the HIJING, AMPT and Saturation models are again compared to the data. While the HIJING and AMPT simulations are in good agreement with experiment, the saturation models predicts a ratio that has a very different pseudorapidity dependence.

It can be noted that by scaling with the total number of d- and Au- participants, the ratio R approaches unity for large, negative pseudorapities(Au-fragmentation side), increases to 25% above unity near midrapidity, and then drops to a relatively low value for large, positive pseudorapidities (d-fragmentation side). The participant ratios appropriate for Au- and d-participant-only scaling are 0.57 and 0.89, which would result in the R values as indicated by the left and right arrows in Fig 2c, respectively. Particle production away from mid-rapidity appears to follow the participant scaling of the respective fragment.

The d+Au system has previously been studied by the NA35 experiment at $\sqrt{s_{NN}} = 19.4$ GeV [16] where data were obtained for both negative hadrons $h^-$and for the net baryons as measured by the difference of proton and antiproton yields $(p - \bar{p})$. Pseudorapidity distributions were developed with an experiment that selected 43% of the total inelastic cross section, with both deuteron nucleons acting as participants. For comparison with the present results, the total charged-particle densities are determined for the lower energy data taking $dN_{ch}/d\eta = 2 \times dN(h^-)/d\eta + dN(p-\bar{p})/d\eta$, where the pseudorapidity densities are deduced from the quoted rapidity distributions by first shifting to the center-of-mass system and then assuming the π^- mass for h^- and the observed mean-p_t values for the h^- and $p - \bar{p}$ distributions. At the higher energy of the current measurement, HIJING model simulations indicate that the criteria that both deuteron nucleons act as participants is well satisfied for the 0-30% centrality range. In this case it is interesting to see if the limiting fragmentation behavior previously observed in Au+Au yields at $\sqrt{s_{NN}} = 130$ and 200 GeV [9, 10] is present in the d+Au system.

Figure 3a compares the d+Au pseudorapidity distri-

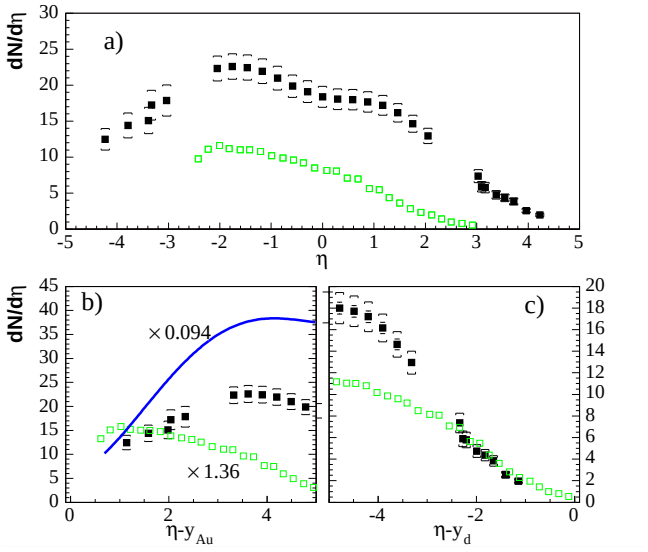

FIG. 3: Comparison of central $\sqrt{s_{NN}} = 200$ GeV results(solid squares) with NA35 data (open squares) at $\sqrt{s_{NN}} = 19.4$ GeV in a) the nucleon-nucleon center-of-mass system, b) the Au rest frame, c) the deuteron rest frame. The solid curve is based on data for Au+Au 0-30% central events at $\sqrt{s_{NN}} = 200$ GeV [10]. N_{part} scaling is applied as indicated in panel b).

butions in the nucleon-nucleon center-of-mass system, where the fixed-target NA35 results have been shifted by the center-of-mass rapidity. The factor of 2.2 increase in charged-particle density at mid-rapidity significantly exceeds the ratio of the total number of participants at the two energies, based on the HIJING simulations, of $\langle N_{part}\rangle(200\text{ GeV})/\langle N_{part}\rangle(19.4\text{ GeV}) = 13.6/10.5 = 1.3$. Fig. 3b compares the data at the two energies in the frame of the Au fragment. Here the NA35 results have been scaled up by the ratio of Au participants at the two energies. The two distributions have similar values approaching the Au rapidity. The solid curve shows the results of the 0-30% central Au+Au distribution at $\sqrt{s_{NN}} = 200$ GeV [10], scaled by the ratio of d+Au gold participants to the number of participant pairs for the Au+Au reaction. The results seem to merge with the d+Au distribution taken at the same $\sqrt{s_{NN}}$ value approaching the Au fragmentation region. The current measurements do not take us close enough to the beam rapidities to claim limiting fragmentation scaling on the Au fragmentation side, although the data, taken together with the earlier results shown in Fig. 2c, may suggest such behavior. Finally, Fig. 3c compares the two d+Au distributions in the deuteron frame. With the given centrality selections, $N_{part}(\text{d}) \approx 2$ at both energies and so no participant scaling is done for the comparison. The two distributions are found to overlap, again suggesting a limiting fragmentation behavior.

We have measured pseudorapidity densities of charged particles for the d+Au reaction at $\sqrt{s_{NN}} = 200$ GeV for different centrality ranges. The ratio of particle densities for central and peripheral events is found to agree well with participant scaling in terms of the respective fragments away from mid-rapidity. At mid-rapidity we find a yield for central collisions that is in excess of that attributable to participant scaling. Overall, model calculations based on both soft physics and perturbative QCD lead to excellent agreement with the experimental results whereas calculations based on the saturation picture using scale parameters set by previous experimental data appear to have difficulty in reproducing the measurements. Comparison with lower energy d+Au data suggest a significant enhancement of the mid-rapidity yields at the higher energy with a limiting fragmentation-like behavior observed near the rapidity of the d and Au fragments.

We thank the RHIC collider team for their efforts. This work was supported by the Office of Nuclear Physics of the U.S. Department of Energy, the Danish Natural Science Research Council, the Research Council of Norway, the Polish State Committee for Scientific Research (KBN) and the Romanian Ministry of Research.

[1] L. V. Gribov, E. M. Levin and M. G. Ryskin, Phys.Rep. **100**, 1 (1983).
[2] K. J. Eskola, K. Kajantie and K. Tuominen, Phys. Lett. **B497**, 39 (2001).
[3] D. Kharzeev and E. Levin, Phys. Lett. **B523**, 79 (2001).
[4] D. Kharzeev and M. Nardi. Phys. Lett. **B507**, 121 (2001).
[5] D. Kharzeev, E. Levin, and M. Nardi, Nucl. Phys. A **730**, 448 (2004).
[6] B. B. Back *et al.*, Phys. Rev. Lett. **85**, 3100 (2000).
[7] C. Adler *et al.*, Phys. Rev Lett. **87**, 112303 (2001).
[8] K. Adcox *et al.*, Phys. Rev. Lett. **86**, 3500 (2001).
[9] I. G. Bearden *et al.*, Phys. Lett. **B523** (2001) 227.
[10] I.G. Bearden *et al.*, Phys. Rev. Lett. **88**, 202301 (2002);
[11] B. B. Back *et al.*, Phys. Rev. Lett.**88**, 022302 (2002).
[12] X. N. Wang and M. Gyulassy, Phys. Rev. D **44**, 3501 (1991); code HIJING 1.383.
[13] Bin Zhang, C. M. Ko, Bao-An Li and Zi-wei Lin, Phys. Rev. C **61**, 067901 (2000).
[14] Zi-wei Lin, Subrata Pal, C. M. Ko, Bao-An Li and Bin Zhang, Phys. Rev. C **64**, 011902R (2001).
[15] Zi-wei Lin, Subrata Pal, C.M. Ko, Bao-An Li and Bin Zhang, Nucl. Phys. **A698**, 375c-378c (2002).
[16] T. Alber *et al.*, Eur. Phys. J. C **2**, 643 (1998).
[17] Y.K. Lee *et al.*, Nucl. Inst. Meth. A **516**, 281(2004).
[18] S. Bültmann *et al.*, Phys. Lett. **B579**, 245 (2004).
[19] M. Adamczyk *et al.*, Nucl.Inst. Meth A **499**, 437 (2003).
[20] GEANT 3.2.1, CERN program library.
[21] B. B. Back *et al.*, submitted for publication (2003); nucl-ex/0311009.